

Short Communication

Optimization of MoS₂-g-C₃N₄ Heterojunction Photocatalyst by NH₃ Plasma Treatment with 2.45 GHz Microwave Source

Daqian Wang¹, Shuchang Xu¹, Xijiang Chang^{1,2*}

¹ College of Science, Donghua University, North Renmin Road 2999, 201620 Shanghai, P. R. China

² Magnetic Confinement Fusion Research Center of Ministry Education, Donghua University, North Renmin Road 2999, 201620 Shanghai, P. R. China

*E-mail: Changxj@dhu.edu.cn

Received: 4 May 2022 / Accepted: 23 June 2022 / Published: 7 August 2022

Microwave surface wave plasma was employed to process surface modification of MoS₂-g-C₃N₄ composite for the purpose of photocatalytic activity enhancement. MoS₂-g-C₃N₄ was synthesized by solvothermal method and plasma processing with different atmospheres have been done. After a variety of material characterization methods, catalytic and electrochemical tests, we found that different plasma surface modification of the material has an impact on all aspects of the characteristics. In Ar plasma processing, the ion bombardment made the MoS₂-g-C₃N₄ surface defects more and decreased the material bandgap. With NH₃ plasma the group functionalization on material can increase the MO dissociation efficiency than that of Ar plasma treated.

Keywords: MoS₂-g-C₃N₄, Plasma, Catalyst, Surface modification, Photodegradation

1. INTRODUCTION

Energy crisis and environmental pollution have become increasingly serious worldwide along with the rapid modern industrialization and population growth. In recent years, MoS₂-g-C₃N₄ is used as an inexpensive, stable visible catalyst owing to its suitable band gap, unique electronic band structure, and high chemical and thermal stability[1-3]. It is widely applied in photocatalytic conversion of solar energy, such as photocatalytic decomposition to produce hydrogen and oxygen, and degradation of organic pollutants[4-7].

Plasma technology is widely used in materials research due to its special properties and its diverse forms, such as plasma-enhanced chemical vapor deposition, ion implantation, plasma etching, plasma polymerization, and surface modification[8-10]. Compared to conventional methods, the complex composition of the plasma provides the sample material an environment with extremely high physical and chemical activity, and surface modification of the material is easier and more effective under such

conditions[11,12]. Owing to its excellent performance for surface modification, plasma treatment can effectively enhance the surface activity and reaction efficiency of MoS₂-g-C₃N₄[13-17].

In this work, we used low-temperature plasma to treat MoS₂-g-C₃N₄, and employed Ar₂ and NH₃ as plasma atmospheres for surface modification of the material, respectively. The plasma-processed materials were characterized systematically by X-ray diffractometry (XRD), Fourier transform infrared (FTIR) spectrometry, X-ray Photoelectron Spectroscopy (XPS), photoluminescence (PL), Electrochemical impedance spectroscopy (EIS), UV-vis diffuse reflectance spectra (DRS) and scanning electron microscopy (SEM) to investigate the effects of different plasma gases on treating MoS₂-g-C₃N₄[18]. The reason of catalytic performance was analyzed from the surface view, which is closely related with the plasma gases[19-21].

2. EXPERIMENTAL SECTION

2.1. Materials

All chemicals including carbon nitride (C₃N₄), thiourea (CN₂H₄S), sodium molybdate (Na₂MoO₄·2H₂O), ethylene glycol ((CH₂OH)₂), methyl orange (MO), and ethanol were of analytical grade. All chemicals were purchased from Xilong Chemical Co., Ltd. (Guangdong, China) and used according to the specifications.

2.2. Synthesis of MoS₂-g-C₃N₄

MoS₂-g-C₃N₄ was synthesized by a solvothermal method using ethylene glycol as the solvent. First, 0.5 g of g-C₃N₄ was dissolved in 25 ml of a (CH₂OH)₂ solution, followed by ultrasonication for 15 minutes. Then 0.13 mmol of Na₂MoO₄·2H₂O and 0.65 mmol of CN₂H₄S were mixed into the solution under ultrasonic treatment, and then magnetically stirred for 1 hour of full mixing. The mixture was collected using a 50 ml reactor and kept in a desiccator at 210 °C for 24 hours. After the reaction, the mixture was centrifuged and then washed twice with deionized water and ethanol, followed by a vacuum desiccator at 80°C for 8 hours. The final dried powder was labeled as MoS₂-g-C₃N₄.

2.3. Plasma Treatment

In the whole plasma device, as shown in Figure 1, a 2.45 GHz microwave source (Muege, 1 kW) drives the plasma generator, which can adjust and monitor both the incident power and reflected power in real time. The microwaves are transmitted in a rectangular waveguide system and coupled to the process via a slit antenna through a quartz plate beneath the waveguide, which is also used as a vacuum seal. At the end of waveguide, a short plunger and 3-stub tuner are used to adjust to the coupling. A two-stage pumping system maintains the vacuum degree in the chamber at 10⁻⁴ Pa. On this basis the different working gases are introduced into the vacuum chamber in the required ratio by means of mass flow controllers (MFCs). During plasma discharging, pressure in the chamber can be set by adjusting a high-

precision valve on the exhaust port. Typically, the samples are placed on a platform 10 cm away from the quartz plate.

For the processing, the pumping system is turned on after the sample has been properly placed to remove any residual air to achieve a preliminary vacuum. The working gas is then introduced as required and the initial discharge pressure was set. When the pressure is stabilized the microwave unit is turned on to generate plasma in the chamber. During the discharge process the air pressure in the chamber is set at around 20Pa, the microwave input power is approximately 800W with reflected power is less than 10%. The plasma conditions for the material treatment are listed in Table 1.

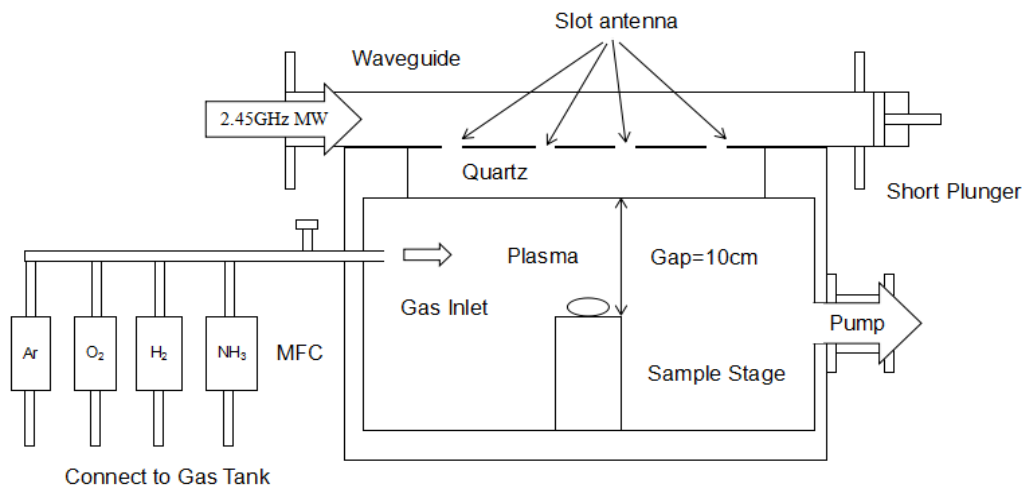


Figure 1. Schematic of the plasma surface modification system

Table 1. Condition of plasma treatment for MoS₂-g-C₃N₄ surface modification

| | |
|--|-----------------------------|
| Total gas flow | 50 sccm |
| Discharge power (2.45GHz Microwave) | 800 W |
| Processing time | 5 min |
| Sample gap (from the discharge region) | 10 cm |
| Initial pressure | 15-25 Pa |
| Working gas | (1) Ar; (2) NH ₃ |

2.4. Material Characterization

After plasma treatment, the MoS₂-g-C₃N₄ samples were sealed to isolate from air. Due to the timeliness of plasma-treated samples, the experiments shall be conducted as soon as possible. FTIR spectra were recorded using a Nicolet AVATAR 370 spectrometer. A D2 PHASER XRD meter was used to determine the crystal structures. Morphology of MoS₂-g-C₃N₄ was observed using an SEM device (Hitachi S-8000, Japan) in a secondary electron scattering mode. PL spectra were recorded on an FS-5 fluorescence spectrophotometer under excitation at 300 nm. UV-vis absorption spectroscopy was

measured on a Shimadzu UV-3600 spectrophotometer. Brunauer-Emmett-Teller (BET) specific surface areas were calculated. X-ray photoelectron spectroscopy (XPS) was measured using an ESCALAB 250 Xi detector.

2.5. Catalysis Application

The catalytic activity of the samples as-prepared were assessed by the degradation of 25 mg/L MO solutions under a 500 W mercury lamp. The photocatalyst (30 mg) was placed in a 30 mL MO solution in a quartz tube. The dye solution was stirred for 70 min in the dark and 90 min in the light according to the pre-set time interval. Then 1.0 mL of the solution was taken out and analyzed with a UV-Vis spectrophotometer at the maximal absorption wavelength of 465 nm (MO).

2.6. Photoelectrochemical Measurement

The electrochemical impedance spectra (EIS) and photocurrent response were measured on an electrochemical workstation (CHI-660D, CHI Shanghai, Inc.). The film samples, Pt sheets, saturated calomel, and a 0.3 M Na₂SO₄ aqueous solution were used as the working electrode, the electrode, the reference electrode and the electrolyte, respectively. To prepare the working electrode, the samples as-prepared (50 mg) were ground with 2 mL of ethanol to form a slurry. Then the slurry was coated onto an F-doped SnO₂-coated glass (FTO glass, 2 × 1.2 cm²) electrode using the doctor blade method. The electrodes were oven-dried at 80 ° C for 30 min[22-24].

3. RESULTS AND DISCUSSION

Two different atmosphere plasmas were employed to process the as-prepared MoS₂-g-C₃N₄ sample. The XRD patterns of pure MoS₂, C₃N₄ and MoS₂-g-C₃N₄ composites were shown in Figure 2. The structure of MoS₂ is in the orthorhombic form (JCPDS Card No. 37 - 1492). The pure g-C₃N₄ exhibits two important peaks around 12.7° and 27.2°, which are characteristic of g-C₃N₄[25,27]. Besides, the MoS₂-g-C₃N₄ reveals similar XRD patterns. For the MoS₂-g-C₃N₄ composite, after the plasma treatment, the diffraction peaks of MoS₂ are apparent in the XRD patterns, and the atmospheric plasma treatments have specific strengths due to the increase of the diffraction peaks of the MoS₂ crystal plane.

Figure 3 shows the FTIR spectra of g-C₃N₄, MoS₂ and MoS₂-g-C₃N₄ synthesized by the chemical method. Clearly, pure g-C₃N₄ and MoS₂-g-C₃N₄ both show obvious infrared peaks of graphite phase carbonitride, and the peaks of 1000 - 1750 cm⁻¹ belong to the C=N and C-N on the nitrogen-carbon heterocyclic compound. The broad absorption peak at 3100 - 3300 cm⁻¹ is attributed to the stretching vibration of the amino group (-NH-)[28]. The infrared spectra of plasma-treated and untreated samples both show a peak shape similar to that of g-C₃N₄. Obviously, the peak intensity of the composite increases and the peak position slightly red-shifts. The plasma treatment enhanced this trends obviously.

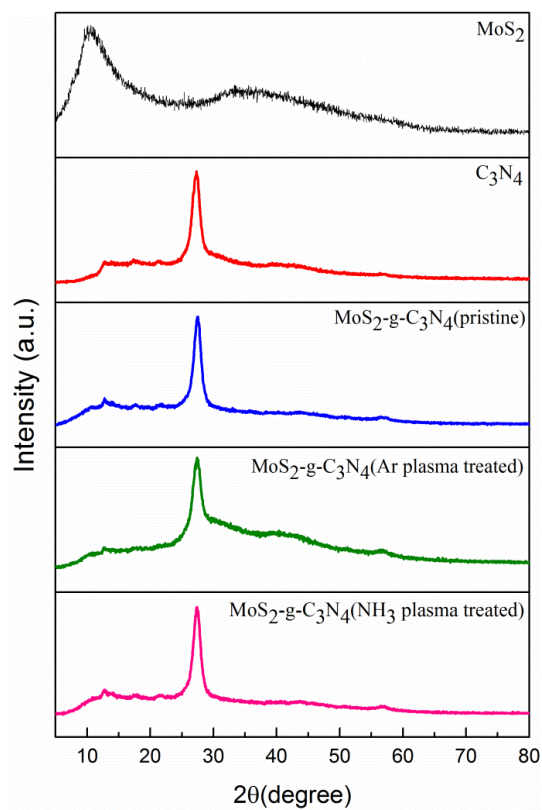


Figure 2. XRD patterns of g-C₃N₄, MoS₂, MoS₂-g-C₃N₄ samples

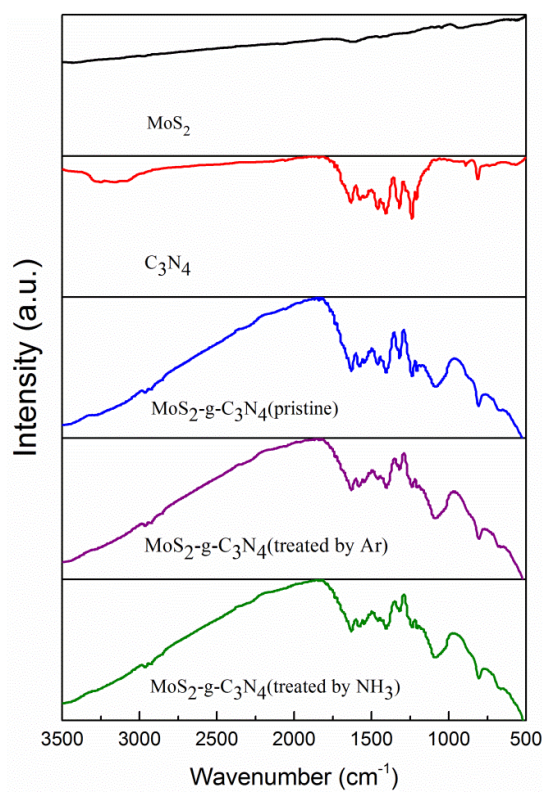


Figure 3. FT-IR spectra of g-C₃N₄, MoS₂, MoS₂-g-C₃N₄

The XPS spectra were collected to investigate the chemical composition and chemical states of the MoS₂-g-C₃N₄ composite. The XPS survey spectra (Figure 4) indicate the presence of C, N, and O in the bulk g-C₃N₄, and C, N, O, Mo, and S in MoS₂-g-C₃N₄. The deconvolution of the XPS C 1s spectrum is shown in Figure 4 (a) [29]. We can find that after the NH₃ plasma treatment, C-N component increased obviously due to the bombardment of N related active radicals in NH₃ plasma. Correspondingly, the MoS₂ component was reduced to some extent due to plasma etching effect, which can be found from the Mo 3d and S 2p.

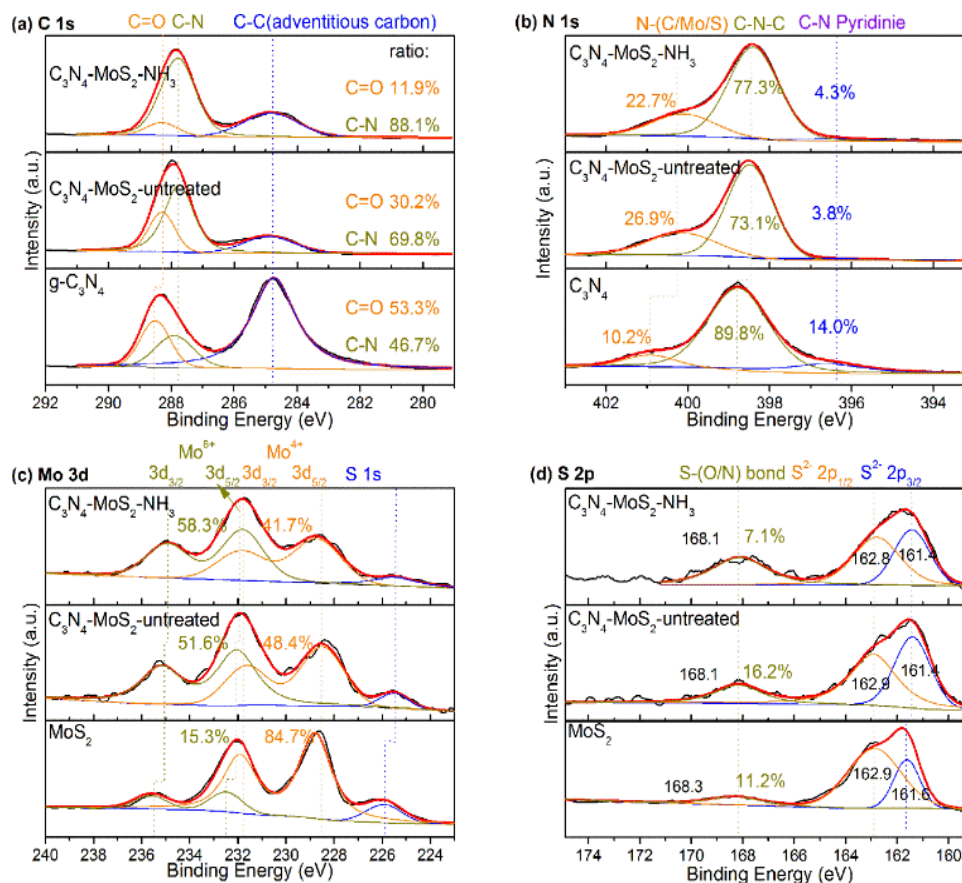


Figure 4. XPS survey spectra of g-C₃N₄, MoS₂, MoS₂-g-C₃N₄

PL spectra can reveal the photogenerated charge transport during the photocatalytic reaction (Figure 5). Theoretically, a higher PL intensity means the carriers participate more efficiently in the recombination, and vice versa. The PL intensity of the pristine MoS₂-g-C₃N₄ is higher than that of the plasma-treated MoS₂-g-C₃N₄. This result means the plasma-treated MoS₂-g-C₃N₄ has weak photogenerated electron and hole recombination efficiency relative to pristine MoS₂-g-C₃N₄, and there is a rapid migration and separation of photogenerated carriers in the plasma-treated MoS₂-g-C₃N₄.

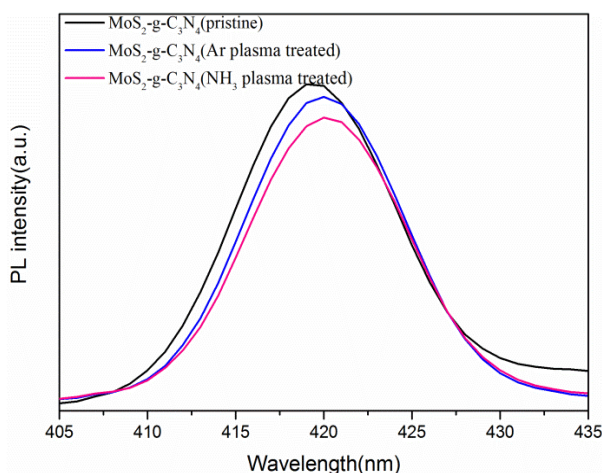


Figure 5. PL spectra of MoS₂-g-C₃N₄

Figure 6 displays the UV-vis diffuse reflectance spectra (DRS) of the pristine MoS₂-g-C₃N₄ and a series of MoS₂-g-C₃N₄ after plasma treatment. The maximum absorption wavelength of pristine MoS₂-g-C₃N₄ is about 415 nm. It has a wide range of visible light absorption, and the absorption intensity in the ultraviolet region is low [29-30] (Figure 6(a)). Compared with plasma-treated MoS₂-g-C₃N₄, the absorption wavelength slightly blue-shifts. The band gap width of plasma-treated MoS₂-g-C₃N₄ composites is smaller than that of the pristine MoS₂-g-C₃N₄ (Figure 6(b)). Because g-C₃N₄ can be induced by visible light excitation to produce electrons and holes on its surface, these electrons possess strong oxidation and reducibility, but are extremely easy to recombine. The electrons and holes can be separated after loading with MoS₂.

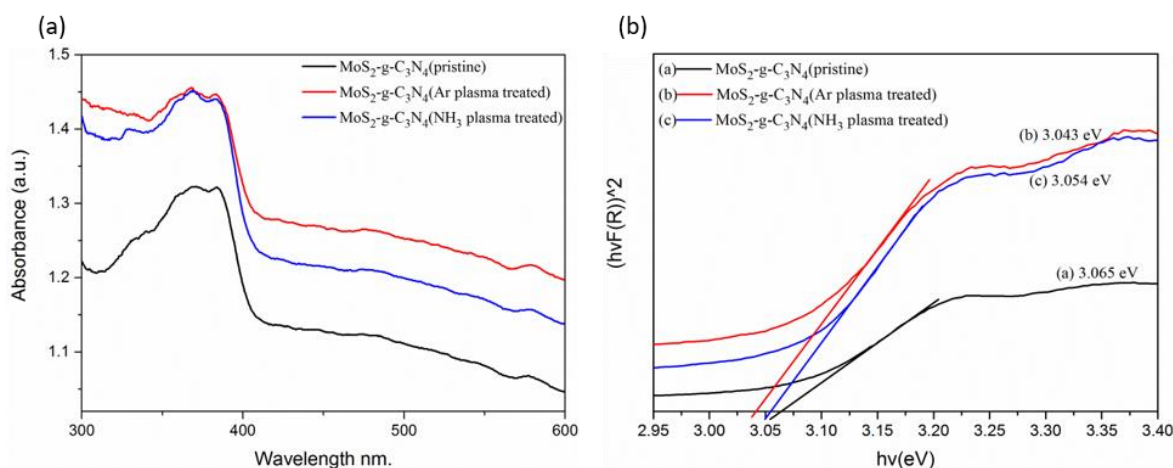


Figure 6. (a) UV-vis DRS of MoS₂-g-C₃N₄; (b) plots of $(h\nu F(R))^2$ versus energy ($h\nu$)

The efficiency of the photoinduced charge separation was examined by the Electrochemical impedance spectroscopy (EIS), and the results are in Figure 7. In general, the surface charge transfer

resistance (R_{ct}) is equivalent to the diameter of semicircle of the Nyquist diagrams and a smaller radius represents the lower resistance for charge transfer. The radius of semicircle increases in the order of $\text{MoS}_2 < \text{MoS}_2\text{-g-C}_3\text{N}_4$ (Ar-plasma-treated) $< \text{MoS}_2\text{-g-C}_3\text{N}_4$ (NH_3 -plasma-treated) $< \text{C}_3\text{N}_4 < \text{MoS}_2\text{-g-C}_3\text{N}_4$ (pristine). Therefore, it can be inferred that the $\text{MoS}_2\text{-g-C}_3\text{N}_4$ composites possess the optimum efficiency in separation and transfer of photoinduced e^-/h^+ pairs.

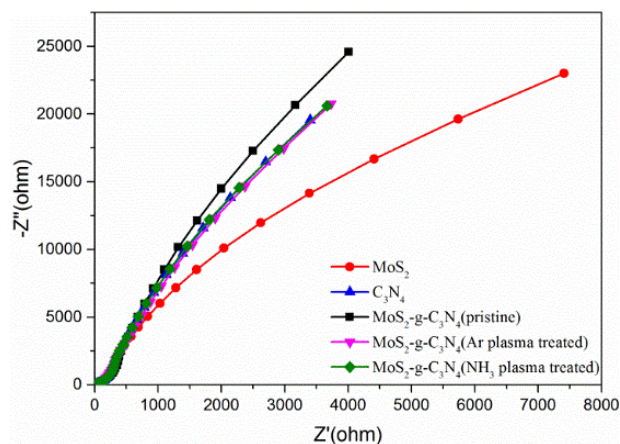


Figure 7. EIS Nyquist plots of curves: MoS_2 , $\text{MoS}_2\text{-g-C}_3\text{N}_4$ (Ar-treated), $\text{MoS}_2\text{-g-C}_3\text{N}_4$ (NH_3 -treated), C_3N_4 , $\text{MoS}_2\text{-g-C}_3\text{N}_4$ (pristine)

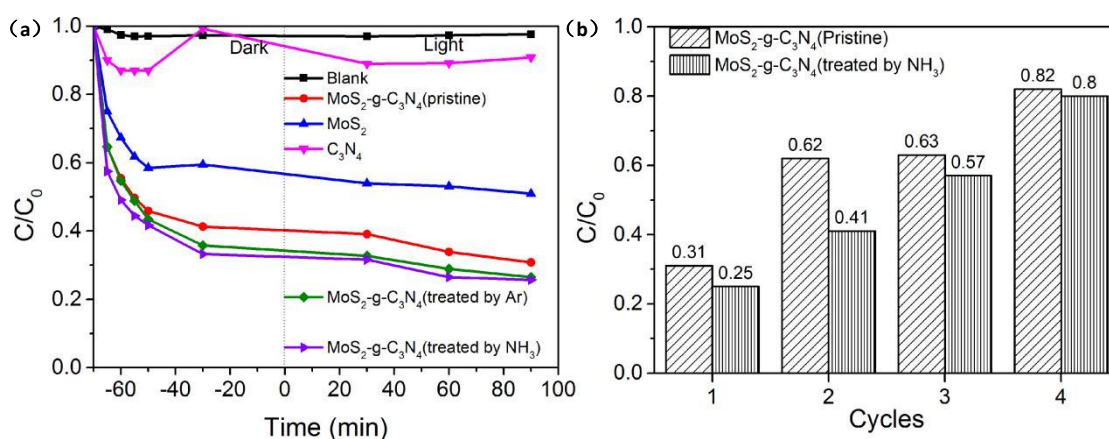


Figure 8. (a) Degradation curves of MoS_2 , $\text{g-C}_3\text{N}_4$, $\text{MoS}_2\text{-g-C}_3\text{N}_4$ (pristine) and $\text{MoS}_2\text{-g-C}_3\text{N}_4$ (NH_3 plasma treatment) on MO solutions; (b) Comparison of $\text{MoS}_2\text{-g-C}_3\text{N}_4$ (pristine) and $\text{MoS}_2\text{-g-C}_3\text{N}_4$ (NH_3 plasma treated) photocatalytic degradation

Figure 8 shows the photoactivity of MoS_2 , $\text{g-C}_3\text{N}_4$, $\text{MoS}_2\text{-g-C}_3\text{N}_4$ (pristine), $\text{MoS}_2\text{-g-C}_3\text{N}_4$ (Ar-plasma-treated), $\text{MoS}_2\text{-g-C}_3\text{N}_4$ (NH_3 -plasma-treated) as well as the mechanism for visible-light-induced photocatalytic performance of the samples toward a 25 mg/L MO solution. The $\text{MoS}_2\text{-g-C}_3\text{N}_4$ samples treated by plasma under NH_3 provided the highest photoactivity and completely degraded MO within 150 min of visible light irradiation. Under the same experimental conditions, the degradation efficiency of MoS_2 , $\text{MoS}_2\text{-g-C}_3\text{N}_4$ (pristine), $\text{MoS}_2\text{-g-C}_3\text{N}_4$ (Ar-plasma-treated), and $\text{MoS}_2\text{-g-C}_3\text{N}_4$ (NH_3 -plasma-treated) is 50%, 30%, 31% and 26%, respectively[31-33]. The higher photocatalytic degradation

efficiency of the MoS₂-g-C₃N₄ samples treated by NH₃ plasma is ascribed to the stronger visible light absorption, higher photocurrent density, and higher efficiency of photoinduced e⁻/h⁺ pair separation and transmission compared with the other samples[31-34].

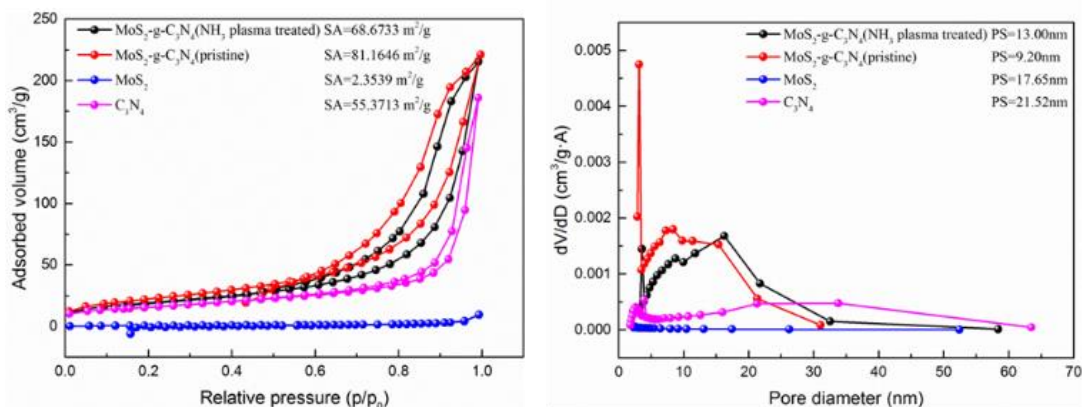


Figure 9. Nitrogen adsorption isotherm and the corresponding curves of the pore diameter distributions of MoS₂, g-C₃N₄, MoS₂-g-C₃N₄ (pristine), MoS₂-g-C₃N₄ (NH₃ plasma treated)

The BET surface area, pore size distributions and the full data of the samples were shown in Figure 9, it can be seen that the BET surface area of MoS₂-g-C₃N₄ (pristine) is 81.16 m²g⁻¹, and of MoS₂-g-C₃N₄ (NH₃ plasma treated) is 68.67 m²g⁻¹, and they are higher than MoS₂ and g-C₃N₄.

4. CONCLUSIONS

Microwave surface wave plasma modification has been done on MoS₂-g-C₃N₄ composite synthesized by solvothermal method. Different plasma atmospheres have been employed and the effect on materials have been evaluated by XRD, FTIR, SEM and PL. Then methyl orange was used as the target degradation agent to analyze the catalytic properties of the composites with/without plasma treatment. We found that plasma treatment can effectively enhance the surface activity and reaction efficiency of MoS₂-g-C₃N₄ composite.

ACKNOWLEDGEMENTS

This research is supported by National Natural Science Foundation of China (No. 12175035).

References

1. S.A. Ansari and M.H. Cho, *Sci. Rep.*, 7 (2017) 1.
2. Y. Cao, Q. Gao, Q. Li, X. Jing, S. Wang and W. Wang, *RSC Adv.*, 7 (2017) 40727.
3. X. Wang, M. Hong, F. Zhang, Z. Zhuang and Y. Yu, *ACS Sustainable. Chem. Eng.*, 4 (2016) 4055.
4. Y. Cao, Q. Li and W. Wang, *RSC Adv.*, 7 (2017) 6131.

5. D. Lu, H. Wang, X. Zhao, K.K. Kondamareddy, J. Ding, C. Li and P. Fang, *ACS Sustainable Chem. Eng.*, 5 (2017) 1436.
6. Z.T. Wang, J. Hasan, J.J. Wang, C.W. Zhang, W. Iqbal, N.H. Chang and C.G. Qin, *J. Nanopart. Res.*, 24 (2022) 83.
7. H. Tran Huu, M.D.N. Thi, V.P. Nguyen, L.N. Thi, T.T.T. Phan, Q.D. Hoang, H.H. Luc, S.J. Kim and V. Vo, *Sci. Rep.*, 11 (2021) 14787.
8. I. Motrescu, A. Ogino, S. Tanaka, T. Fujiwara, S. Kodani, H. Kawagishi, G. Popa and M. Nagatsu, *Thin Solid Films*, 518 (2010) 3585.
9. K. Sasai, H. Suzuki and H. Toyoda, *Jpn. J. Appl. Phys.*, 55 (2016) 016203.
10. L. Wang, Q.D. Chen, X.W. Cao, R. Buividas, X. Wang, S. Juodkazis and H.B. Sun, *Light: Sci. Appl.*, 6 (2017) 7.
11. J.G. Alonso, C. Dalmolin, J. Nahorny, A.A. Recco, L.C. Fontana and D. Becker, *Journal of Polymer Engineering*, 38 (2018) 795.
12. B. Miao, Y. Chai, K. Wei and J. Hu, *Vacuum*, 133 (2016) 54.
13. B. Wang, B. Chen, Y. Sun, H. Xiao, X. Xu, M. Fu, J. Wu, L. Chen and D. Ye, *Appl. Catal., B*, 238 (2018) 328.
14. X. Wang, Y. Chen, M. Fu, Z. Chen and Q. Huang, *Chin. J. Catal.*, 39 (2018) 1672.
15. X. Zhang, W. Xu, D. Duan, D.W. Park and L. Di, *IEEE Trans. Plasma Sci.*, 46 (2018) 2776.
16. J. X. Zheng, B. Zhang and Z. Wang, *RSC Adv.*, 11 (2021) 78.
17. B. Zhang, Z.H. Wang, X.F. Peng, Z. Wang, L. Zhou and Q.X. Yin, *Nanomaterials*, 9 (2019) 1139.
18. B. Xue, H.Y. Jiang, T. Sun, F. Mao and J.K. Wu, *Mater. Lett.*, 228 (2018) 475.
19. X. Lu, Y. Jin, X. Zhang, G. Xu, D. Wang, J. Lv, Z. Zheng and Y. Wu, *Dalton Trans.*, 45 (2016) 15406.
20. W.C. Peng and X.Y. Li, *Catal. Commun.*, 49 (2014) 63.
21. Y. Tian, L. Ge, K. Wang and Y. Chai, *Mater. Charact.*, 87 (2014) 70.
22. H.R. An, Y.C. Hong, H. Kim, J.Y. Huh, E.C. Park, S.Y. Park, Y. Jeong, J.I. Park, J.P. Kim, Y.C. Lee, W.K. Hong, Y.K. Oh, Y.J. Kim, M. Yang and H.U. Lee, *J. Hazard. Mater.*, 358 (2018) 222.
23. X.C. Kong, Y.M. Xu, Z.D. Cui, Z.Y. Li, Y.Q. Liang, Z.H. Gao, S.L. Zhu and X.J. Yang, *Appl. Catal., B*, 230 (2018) 11.
24. Z.D. Mahmoudabadi, E. Eslami and M. Narimisa, *J Colloid Interface Sci.*, 529 (2018) 538.
25. P. Fageria, K.Y. Sudharshan, R. Nazir, M. Basu and S. Pande, *Electrochim. Acta*, 258 (2017) 1273.
26. H. Fan, R. Wu, H. Liu, X. Yang, Y. Sun and C. Chen, *J. Mater. Sci.*, 53 (2018) 10302.
27. B. Peng, P.K. Ang and K.P. Loh, *Nano Today*, 10 (2015) 128.
28. M.H. Wu, L. Li, Y.C. Xue, G. Xu, L. Tang, N. Liu and W.Y. Huang, *Appl. Catal., B*, 228 (2018) 103.
29. N. Liu, W. Huang, X. Zhang, L. Tang, L. Wang, Y. Wang and M. Wu, *Appl. Catal., B*, 221 (2018) 119.
30. H. Yan, X. Wang, M. Yao and X. Yao, *Prog. Nat. Sci.: Mater. Int.*, 23 (2013) 402.
31. T. Araya, M. Jia, J. Yang, P. Zhao, K. Cai, W. Ma and Y. Huang, *Appl. Catal., B*, 203 (2017) 768.
32. C. Byrne, G. Subramanian and S.C. Pillai, *J. Environ. Chem. Eng.*, 6 (2018) 3531.
33. V. Etacheri, C. Di Valentin, J. Schneider, D. Bahnemann and S.C. Pillai, *J. Photochem. Photobiol., C*, 25 (2015) 1.
34. W. Fu, H. He, Z. Zhang, C. Wu, X. Wang, H. Wang, Q. Zeng, L. Sun, X. Wang and J. Zhou, *Nano Energy*, 27 (2016) 44.